

AIAA 2002-0481
EXPERIMENTAL AND NUMERICAL INVESTIGATION
OF PREMIXED CYLINDRICAL FLAMES

D. Mosbacher, J. Wehrmeyer, R. Pitz
Mechanical Engineering Department
Vanderbilt University
Nashville, TN 37235

C.-J. Sung
Mechanical and Aerospace Engineering Department
Case Western Reserve University
Cleveland, OH 44106

J. Byrd
Engineering Technology Department
Austin Peay State University
Clarksville, TN 37044

EXPERIMENTAL AND NUMERICAL INVESTIGATION OF PREMIXED CYLINDRICAL FLAMES

D. Matt Mosbacher,* Joseph A. Wehrmeyer,[†] Robert W. Pitz[¶]
Mechanical Engineering Dept., Vanderbilt University, Nashville, TN 37235

C.-J. Sung^Ω
Mechanical & Aerospace Engineering Dept., Case Western Reserve University, Cleveland OH 44106

John L. Byrd[§]
Engineering Technology Dept., Austin Peay State University, Clarksville, TN 37044

Abstract

Fundamental flame response in a stretched and curved flow-field is investigated in a unique optically accessible tubular burner. Time-averaged, one-dimensional spatially-resolved temperature and major species measurements are obtained in a set of stretched, $\phi = 0.175$ premixed H₂-air tubular flames using visible laser-induced Raman spectroscopy. The very lean H₂-air flames are formed under relatively high stretch rates, $90 \leq k \leq 215 \text{ s}^{-1}$, with 227 s^{-1} being the extinction condition. In tubular flames, both aerodynamic straining and flame curvature determines stretch rate (i.e., thermal-diffusive) effects. Thermal-diffusive effects in highly curved (~1-2 mm flame radius) tubular flames significantly influence flame structure: leading to flame temperature increases of ~120 K over the planar unstretched flame temperature (~1180 K). The standard program for modeling stretched planar flames (Oppdif) is modified for the cylindrical geometry of the tubular flame. Comparisons of the Raman measurements with numerical simulations for tubular premixed flames, using complex chemistry and detailed transport properties, show excellent agreement at low rates of stretch (i.e. $k \leq 127 \text{ s}^{-1}$). At higher flame stretch (increased curvature) simulations using the currently available transport data and chemical mechanisms incorrectly predict tubular flame structure. Experimental observations show extinction occurring, while numerical simulations over-predict the extinction limit.

* Graduate Student

[†] Research Associate Prof., Senior Member, AIAA

[¶] Prof. and Department Chair, Associate Fellow AIAA

^Ω Assistant Professor, Senior Member, AIAA

[§] Assistant Professor

Copyright © 2002 by D. Mosbacher. Published by the American Institute of Aeronautics and Astronautics, Inc. with permission

Simulations using four different H₂-air chemical kinetic mechanisms show that flame structure is very sensitive to the particular mechanism and the molecular diffusion coefficients. Evaluation of the molecular diffusion coefficients indicates that the thermo-diffusive properties of the deficient reactant species, H₂, strongly affect the tubular flame structure.

Introduction

Flame-flow interaction is a fundamental problem of interest in combustion research. Experimentally, burners using a variety of flow-fields have been used to study flame behavior: e.g., Bunsen flames [1], counterflow stagnation flames [2], slot-burner flames [3,4], etc. In these burners, the effects of both stretch and curvature on flame behavior have been investigated. Theoretically, the effects of curvature and stretch have been examined under turbulent [5,6] and laminar conditions [7-9]. However, quantitatively evaluating the effects of stretch and curvature in these flames has proved difficult because typically the stretch rates and degree of curvature are small and vary across the flame front. Most of the quantitative work on flame-flow interaction has concentrated on stretched premixed laminar planar flames produced between two counterflowing coaxial jets (opposed jets) [e.g: 10,11]. In this flow configuration, the flow-field only interacts with the one-dimensional flame sheet through aerodynamic straining.

In this work, a unique optically accessible counterflow stagnation burner with cylindrical geometry produces curved (tubular) flames under high rates of stretch. The tubular flame is a geometrical conversion of the twin counterflow flame: i.e., it is a stretched flame, but its cross-

sectional shape is cylindrical [12]. Tubular flames exhibit the same stretch effects observed in planar flames, but with amplification due to curvature. Thus, stretch and thermo-diffusive effects are related to the degree of curvature of the tubular flame. If $Le \neq 1$ (where Le , Lewis number, = thermal diffusivity, α , over the mass diffusivity, D) for the incoming reactant mixture, the local flame temperature responds according to the coupled effects of aerodynamic straining, flame curvature, and Le (or multiple Le 's) [6-9,12]. The changes in flame structure depend upon whether the flame curvature is concave or convex to the incoming reacting mixture. A premixed flame sheet can possess a local temperature above or below the adiabatic flame temperature because of the "focusing" or "defocusing" due to curvature, of both heat release and the molecular diffusion of the deficient reactant.

Premixed tubular flames have been previously examined both experimentally and numerically. Using a rotating flow burner similar to Ishizuka [13], Yamamoto et al. [14] have experimentally investigated tubular premixed flames created in a low stretch vortex. Sakai and Ishizuka [15] and Ogawa et al. [16] injected premixed reactants radially inward through the walls of an open porous cylindrical tube to examine curvature effects at low rates of stretch. Using a burner that directed premixed reactants radially inward completely around the flame circumference, Kobayashi and Kitano [17] examined the extinction characteristics of propane-air and methane-air premixed tubular flames at high rates of stretch and compared them to similar opposed jet flames. Tubular premixed flames have been analyzed numerically in order to predict flame structure and extinction as functions of the inlet velocity boundary condition [18-21]. In these previous studies, the experimental measurements in the tubular flames were limited as the burners had minimal optical access.

Tubular Burner

The tubular burner, as shown in Fig. 1, is similar to that of Ref. 17. A premixed combustible mixture is introduced to the outer circular chamber via a plenum with 16 circumferentially spaced inlet ports. The reactant mixture diffuses through fine gauge (00) stainless steel wool (used to provide a uniform radial

pressure drop in the flow chamber) and exits through a converging cylindrical nozzle of 1.5 cm radius and 2 cm height. A premixed tubular flame, with products exiting radially inward from the flame and the reactants flowing radially inward toward the flame, is formed around the cylindrical axis of the burner. The flame location is the radial position where the burning velocity balances with the upstream radial velocity of the unburned mixture. In this manner, premixed tubular flames of various radii can be formed by adjusting the reactant mixture velocity, thus controlling the degree of curvature and aerodynamic straining.

The axisymmetric flow-field in the tubular burner radially converges and axially diverges. Consequently, the tubular flame is stabilized by a finite rate of stretch. The influence of aerodynamic straining and curvature on flame stretch is determined by evaluating an invariant expression for stretch in a stationary flame [22]. A specific expression for the global stretch rate, k , in the tubular flame can be derived from this expression and is given as

$$k \equiv \frac{2V}{R}, \quad (1)$$

where V is the radial inlet velocity, and R is the nozzle radius (1.5 cm).

A unique feature of the tubular burner is the provision of three optical access ports. Two laser access ports, located at 180° from each other, are 25 mm in diameter. A third 50 mm diameter optical port, located at right angles to the laser ports, is used by the light detection system to collect scattered light. Additionally, co-flow nitrogen ports circumferentially around the two tubular burner exits help stabilize the tubular flame by shielding it from the ambient air. The co-flow nitrogen, also significantly reduces the amount of unstretched combustion outside the tubular burner. Water-cooling jackets, located around the top and bottom of the tubular burner, prevent preheating of the reactant mixture. The axis of symmetry of the burner and its flame is vertically orientated.

Experimental System

A schematic of the experimental system is shown in Fig. 2. Visible laser Raman

spectroscopy is used to measure temperature and species concentrations through the flame. The Raman signals are created by a frequency doubled, pulsed (10 Hz) Nd-YAG (532 nm) laser. The laser output is focused to a beam waist of ~ 0.25 mm to improve spatial resolution transverse to the laser beam. Due to losses from a mirrors-beamsplitter arrangement used to prevent laser-induced breakdown at the laser focus by lengthening the effective pulse length from 7 ns to ~ 35 ns, the energy output of the laser is limited to ~ 225 mJ/pulse.

The Raman scattered light is collected at 90° to the laser beam using a 75 mm diameter F/2 achromat and relayed by another lens into a modified single grating spectrograph [23]. The light detector is a cryogenically cooled, back-illuminated CCD array (1024 x 1024 pixels), allowing one-dimensional spatially resolved time-averaged measurements of Raman signals from all major species. The measured spatial resolution of the imaging system is ~ 120 μm along the 4.6 mm imaged length of the laser.

A 2.5 mm thick OG-550 colored-glass filter and an infrared filter are mounted in series at the entrance slit to minimize the amount of 532 nm and stray infrared light entering the spectrograph. To efficiently gate the camera and reduce time-continuous background flame luminosity, a 44 μs ferroelectric liquid crystal (FLC) is used in series with a 6 ms mechanical shutter at the spectrometer entrance slit, with both open only during the laser pulse. A total of 600 single-pulse Raman images are averaged on the CCD. For the Raman measurements, the laser beam passes through the radial centerline of the flame tube. Based on the spatial resolution of the system, each integrated line-wise image provides ~ 38 useable measurement points. For each flame examined, the burner was translated once to record the flame structure on both sides burner axis. Figure 3 shows a set of Raman spectra obtained in a tubular flame.

The experimental measurements are derived from the Raman signals through an experimental calibration of the Raman system, using several calibration flames produced in a "Hencken" multi-element flat-flame diffusion burner. The ideal gas law is used to relate measured total number density to temperature assuming atmospheric pressure. For calibration

conditions, fuel and air-flow rates were measured with mass flow meters with accuracies of $\pm 1\%$ of their full scale. The accuracy of the temperature measurements, $\pm 2.5\%$, was evaluated by comparing experimental Raman temperature measurements from H_2 -air calibration flames with adiabatic flame temperatures based on measured reactant flowrates.

Numerical Simulations

In order to numerically model premixed tubular flames, the standard Oppdif [24] program was modified to account for the radial geometry. Oppdif normally models opposed jet flames of axial symmetry, where the reactants originate along the symmetry axis and exit radially away from the axis. Flame structure is then mapped onto the axial dimension. In a tubular flame, the radial coordinate, instead of the axial coordinate, is used as the spatial dimension through which flame structure is mapped. By transforming the spatial coordinate and seeking a similarity solution of the two-dimensional conservation equations, the tubular flame can be modeled as a two-point boundary value problem. The Oppdif program was modified for the tubular flame geometry, and the resulting set of differential equations for the cylindrical flame are given in Ref. 20.

Numerical simulations for the experimental premixed H_2 -air tubular flames examined were performed with detailed transport and complex chemistry. Molecular transport properties were determined from mixture-averaged multicomponent calculations using Chapman-Enskog collision theory, Lennard-Jones potentials, and reference data from the CHEMKIN [24] transport database. H_2/O_2 chemical kinetic mechanisms from Mueller et al. [25], Yetter et al. [26], Peters [27], and the relevant H_2/O_2 reactions in GRI-MECH 3.0 [28] were used to investigate flame structure response to chemistry, with these mechanisms using 19, 19, 17, and 25 reversible elementary reactions, respectively, all with 9 chemical species. Thermochemical properties were determined from the CHEMKIN thermodynamic database, except for recommendations provided in the chemistry mechanisms. Gas phase radiation in the optically-thin limit was assumed, using the Planck mean absorption coefficients obtained from Refs. [29,30].

Results and Discussion

To investigate the effects of curvature at various degrees of stretch ($90 \leq k \leq 215 \text{ s}^{-1}$), a set of lean premixed H_2 -air tubular flames ($Le < 1$) at $\phi = 0.175$ were measured. Figure 4 shows a comparison of Raman temperature measurements with numerical simulations using the four different chemical kinetic reaction mechanisms [25-28] including thermal diffusion effects. Data from both sides of the tubular flame centerline are plotted versus radius to illustrate the axisymmetric structure of the flame. The adiabatic equilibrium flame temperature is also shown by the horizontal line at $\sim 875 \text{ K}$ to emphasize diffusive effects. Figure 4 is for a flame with a stretch rate of 90 s^{-1} and measured temperature of $\sim 1295 \text{ K}$, which is $\sim 420 \text{ K}$ above the adiabatic flame temperature. Comparison of the mechanisms reveals that the kinetics of Mueller et al. and Yetter et al. are the strongest, leading to higher flame speeds, larger flame radii, less fuel focusing, and lower flame temperatures. Reaction mechanism trends illustrated in Fig. 4 are representative of all the stretch rates examined. The Mueller et al. and Yetter et al. mechanism predict similar trends; however, the Mueller et al. mechanism, which uses more recently reported reaction rate data, is used in the remainder of the numerical simulations. The predicted flame radius, $\sim 2.1 \text{ mm}$, and temperature, $\sim 1310 \text{ K}$, using the Mueller et al. chemistry (with the correction for thermal diffusion) is in good agreement with the Raman measurements. Only slight differences are seen between prediction and measurement. Predicted flame radius is slightly smaller and measured temperatures show a slight decrease near the flame centerline, possibly due to radiation heat loss. However, numerical simulations that include radiation heat loss predict a negligible loss in temperature of $\sim 2 \text{ K}$, due the lean operating condition.

Figures 5-7 show comparisons of Raman temperature and species concentrations measurements for tubular flames of $k = 90, 127,$ and 190 s^{-1} , respectively. Numerical simulations using the Mueller et al. chemistry mechanism with inclusion of thermal diffusion show good agreement for $\text{H}_2, \text{N}_2, \text{H}_2\text{O},$ and O_2 profiles in Figs. 5 and 6. Convolution of the data from spatial averaging is minimal because of the relatively

“thick” flames studied herein, and hence the spatial resolution used to analyze the spectra, $120 \mu\text{m}$, adequately resolves the flame.

At higher stretch rates ($k > 127 \text{ s}^{-1}$), seen in Fig. 7, incomplete reaction occurs in the experiments as indicated by the reduced flame temperature ($\sim 1185 \text{ K}$) and H_2O mole fraction. The numerical predictions are not in agreement with the experiments and overpredict the temperature by $\sim 180 \text{ K}$. Use of other chemical mechanisms [26-28] does not improve the comparison. Thus, improvements to the chemical kinetic mechanisms are needed to more accurately model lean-limit highly stretched tubular flames.

The effects of thermal diffusion for a $k = 90$ and 190 s^{-1} tubular flame are shown in Figs. 8 and 9, respectively. If the thermal diffusion correction is not included in the simulation for the $k = 90 \text{ s}^{-1}$ flame, the flame temperature ($\sim 1285 \text{ K}$) and radius ($\sim 1.5 \text{ mm}$) are underpredicted. However, as illustrated in Fig. 9, incomplete reaction occurs at higher stretch rates (as indicated in Fig. 7) and the numerical simulations with and without inclusion of the thermal diffusion correction grossly overpredict flame temperature and radius. The results in Figs. 8 and 9 suggest that the increased mass flux of H_2 , or light species, with increasing temperature due to thermal diffusion and diffusive focusing is important in high temperature-gradients characteristic of tubular flames.

Figures 8 and 9 also show the importance of diffusive focusing of H_2 in the tubular flame. The binary diffusion coefficient for H_2 was increased/decreased by decreasing/increasing by $\sqrt{2}$ the Lennard-Jones collision diameter. When the binary diffusion coefficient of H_2 into N_2 is increased/decreased $+32\%/-29\%$, the flame temperature changes $+50\text{K}/-60 \text{ K}$ and $+66/-79 \text{ K}$ and the flame radius changes by $+18\%/-22\%$ and $+22\%/-23\%$, for the $k = 90$ and 190 s^{-1} flames respectively. Due to the focusing effect from curvature, enhancing the diffusion of H_2 causes the flame to become a richer stronger flame, while the opposite occurs for reducing H_2 diffusion. Additionally, enhancing or reducing $\text{H}, \text{H}_2\text{O},$ and OH diffusion has minimal effect on the premixed tubular flame structure, i.e., $\sim \pm 3 \text{ K}$ and no change in flame radius.

The thermal-diffusive effects in Figs. 8 and 9 illustrate the sensitivity of the tubular flame to the transport data. Further improvements in the numerical simulations can be made by implementing more current transport packages as they become available. Paul [32] demonstrated the inaccuracies of the current CHEMKIN package by comparing predicted transport properties as functions of temperature with experimental data. Furthermore, replacing the stiff $1/r^{12}$ repulsive term in the Lennard-Jones potential with an exponential repulsive term can improve the accuracy of the calculated transport properties of species with low molecular weights over a broader range of temperature, 50-2200 K [32].

The coupled effect of stretch and curvature in tubular flames is shown in Fig. 10 by plotting the variations in numerically predicted and measured flame temperatures and radii versus stretch. Flame radius is taken as the distance from the stagnation centerline of the flame to the half-maximum of the temperature profile. Examination of Fig. 10 reveals that H_2 -air tubular flames of $\phi = 0.175$ decrease in radius from ~ 2.25 - 1.05 mm as stretch is increased and extinction occurs at ~ 227 s^{-1} when the flame thickness becomes on the order of the flame radius. Measured and predicted flame temperatures and flame radii vary linearly with stretch. At low stretch rates (decreased curvature), $k \leq 127$ s^{-1} , the flame freely adjusts to the flow conditions, resulting in large flame radius and minor flame temperature responses. However, at increased stretch rates (increased curvature), $k > 127$ s^{-1} , the increased aerodynamic straining pins the tubular flame near the stagnation centerline: dissipating heat and driving extinction [6,9,12,17].

Figure 10 illustrates that curvature effects control flame structure at low stretch, $k \leq 127$ s^{-1} , while aerodynamic straining effects are dominant at higher stretch rates. The numerical simulations accurately predict this curvature/aerodynamic straining transition for flame radius but not for flame temperature. At high rates of stretch, $k > 127$ s^{-1} , numerical simulations do not correctly predict the Karlovitz number, Ka (the ratio of the hydrodynamic time to the chemical time): i.e., when extinction occurs as Ka approaches unity. Additionally, examining the slope of measured and predicted flame thickness in Figs. 8 and 9 and extinction characteristics in Fig. 10 indicate that

transport errors are minor compared to uncertainties in flame chemistry. In investigations of flame/stretch interactions in premixed spherical flames, similar discrepancies between experimental measurements and numerical simulations have been reported [33,34].

The influence of curvature on thermal-diffusive effects is also shown in Fig. 10 by comparing the tubular flame results with numerical predictions of opposed jet planar flames. Simulations of the opposed jet flames, using the tubular flame boundary velocities and a nozzle separation distance of $2R$ (thus keeping the stretch rates the same between the planar and tubular flame cases), were made with Oppdif. The adiabatic equilibrium flame temperature is also shown for reference. Numerical simulations of the opposed jet flame indicate that flame structure is relatively insensitive to aerodynamic straining, due to the propagation nature of the premixed flame [9]. For opposed jet flames from $k = 10$ to 90 s^{-1} , the flame temperature increases ~ 30 K followed by a ~ 30 K decrease from $k = 90$ to 215 s^{-1} . In the low stretch limit, $k \leq 127$ s^{-1} , curvature enhanced thermal-diffusive effects in the tubular flame increase the flame temperature $\sim 10\%$ (120 K) over the planar opposed jet flame, at the same stretch rate, ~ 1180 K. As k decreases, the tubular flame approaches the planar limit and curvature effects diminish. Thus, indicating that, for $Le \leq 1$ mixtures, the tubular flame is stronger than the opposed jet flame due to flame curvature [17, 35].

Conclusions

A unique optically accessible tubular burner has been developed that allows the use of non-intrusive laser diagnostics. Using visible Raman scattering, complete major species concentrations and temperature profiles have been measured in a set of highly stretched lean limit premixed hydrogen-air tubular flames. The premixed hydrogen-air tubular flames formed in this burner have flame temperatures that are ~ 120 K (10%) above the planar unstretched flame temperature (1180 K) due to curvature enhanced thermal-diffusive effects. Sensitivity of the flame structure to the chemical kinetic mechanism and molecular transport data has been demonstrated by comparing the Raman-derived measurements with numerical simulations. Comparisons of measured

temperature and major species concentrations profiles with numerical simulations are in good agreement for flames of low stretch ($k \leq 127 \text{ s}^{-1}$). At these conditions, the molecular transport data and chemical kinetic mechanism are capable of predicting the structure of the H_2 -air tubular flame. The thermo-diffusive properties of the deficient reactant species, H_2 , are shown to be significant in determining the structural characteristics of the tubular flame, while the properties of other radical species (e.g., H , HO_2 , OH) exhibit little influence. At higher flame stretch, hence increased curvature, the numerical simulations using the currently available transport data and chemistry mechanisms overpredict flame temperature and flame radius. As discussed, the inability of the numerical simulations to correctly predict flame structure in lean premixed highly stretched and curved H_2 -air flames, where thermal-diffusive effects are dominant, suggests that a more detailed investigation of the low and intermediate temperature chemistry and transport data is warranted.

Acknowledgements

The authors would like to acknowledge the U.S. Department of Energy's Office of Basic Energy Sciences who has supported this work through a Partnerships for Academic-Industrial Research, PAIR, grant (#DE-FG02-98ER14915, with Dr. Alan H. Laufer as Technical Monitor).

References

- Law, C. K., Ishizuka, S., and Cho, P., *Combust. Sci. Technol.* 28:89 (1982).
- Barlow, R. S., Karpetis, A. N., Frank, J. H., and Chen, J. Y., *Combust. Flame* 127:2102 (2001).
- Choi, C. W. and Puri, I. K., *Combust. Flame* 126:164 (2001).
- Echekki, T. and Mungal, M. G., *Proc. Combust. Inst.* 23:455 (1990).
- Echekki, T. and Chen, J. H., *Combust. Flame* 106:184 (1996).
- Poinsot, T., Veynante, D., and Candel, S., *J. Fluid Mech.* 228:561 (1991).
- Buckmaster, J. D. and Crowley, A. B., *J. Fluid Mech.* 131:341 (1983).
- Mikolaitis, D. W., *Combust. Flame* 57:25 and 58:23 (1984).
- Law, C. K. and Sung, C. J., *Prog. Energy Comb. Sci.* 26:459 (2000).
- Tanoff, M. A., Smooke, M. D., Osborne, R. J., Brown, T. M., and Pitz, R. W., *Proc. Combust. Inst.* 26:1121 (1996).
- Sung, C. J., Liu, J. B., and Law, C. K., *Combust. Flame* 106:168 (1996).
- Ishizuka, S., *Prog. Energy Combust. Sci.* 19:187 (1993).
- Ishizuka, S., *Combust. Flame* 75:367 (1989).
- Yamamoto, K., Ishizuka, S., and Hirano, T., *Proc. Combust. Inst.* 25:1399 (1994).
- Sakai, Y. and Ishizuka, S., *JSME Int. J.* 34:234 (1991).
- Ogawa, Y., Saito, N., and Liao, C., *Proc. Combust. Inst.* 27:3221 (1998).
- Kobayashi, H. and Kitano, M., *Combust. Flame* 76:285 (1989).
- Nishioka, M., Inagaki, K., Ishizuka, S., and Takeno, T., *Combust. Flame* 86:90 (1991).
- Libby, P., Peters, N., and Williams, F., *Combust. Flame* 75:265 (1989).
- Smooke, M. D. and Giovangigli, V., *Proc. Combust. Inst.* 23:447 (1990).
- Ju, Y., Matsumi, H., Takita, K., and Masuya, G., *Combust. Flame* 116:580 (1999).
- Matalon, M., *Combust. Sci. and Technol.* 31:169 (1983).
- Osborne, R. J., Skaggs, P. A., and Pitz, R. W., 34th Aerospace Sciences Meeting Paper No. 96-0175 (1996).
- Kee, R. J., Rupley, F., Miller, J., Coltrin, M., Grcar, J., Meeks, E., Moffat, H., Lutz, A., Dixon-Lewis, G., Smooke, M., Warnatz, J., Evans, G., Larson, R., Mitchell, R., Petzold, L., Reynolds, L., Caracotsios, M., Stewart, W., and Glarborg, P., *User Manual, The CHEMKIN Collection III* (1999).
- Mueller, M. A., Kim, T. J., Yetter, R. A., and Dryer, F., *Int. J. Chem. Kin.* 31:113 (1999).
- Yetter, R. A., Dryer, F. L., and Rabitz, H., *Combust. Sci. Technol.* 79:97 (1991).
- Yetter, R. A., Dryer, F. L., and Rabitz, H., *Combust. Sci. Technol.* 79:97 (1991).
- Peters, N. (1993), *Reduced Kinetic Mechanisms for Applications in Combustion Systems*, (N. Peters and B. Rogg, Eds.) Chapters. 1,5, Springer-Verlag, Berlin (1993).
- Smith, G. P., Golden, D. M., Frenklach, M., Moriarty, N. W., Eiteneer, B., Goldenberg, M., Bowman, C. T., Hanson, R. K., Song, S.,

- Gardiner, W. C., Lissianski, V. V., and Qin, Z., http://www.me.Berkeley.edu/gri_mech/
29. Rothman, L. S., Gamachee, R. R., Tipping, R. H., Rinsland, C. P., Smith, M. A. H., Benner, D. C., Devi, V. M., Flaud, J. M., Peyret, C. C., Perrin, A., Goldman, A., Massie, S. T., Brown, L. R., Toth, R. A., *J. Quant. Spectrosc. Radiat. Trans.* 48:469 (1992).
 30. Soufiani, A. and Taine, J., *Int. J. Heat Mass Trans.* 40:987 (1997).
 31. Kim, T. J., Yetter, R. A., and Dryer, F. L., *Proc. Combust. Inst.* 25:759 (1994).
 32. Paul, P. H., "DRFM: A New Package for the Evaluation of Gas-Phase-Transport Properties," Sandia Report SAND98-8203.
 33. Kwon, O. C. and Faeth, G. M., *Combust. Flame* 124:590 (2001).
 34. Wu, M. S., Ronney, P. D., Colantonio, R. O., and Vanzandt, D. M., *Combust. Flame* 116:387 (1999).
 35. Kobayashi, H. and Kitano, M., *Combust. Sci. Technol.* 75:227 (1991).

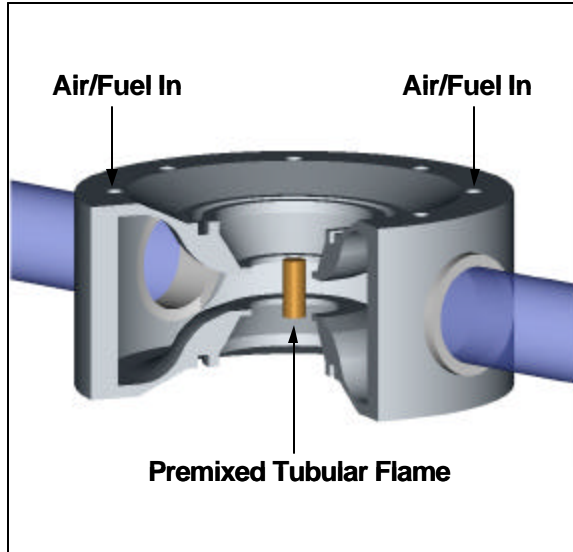


Fig. 1. Schematic of radial counterflow tubular burner design.

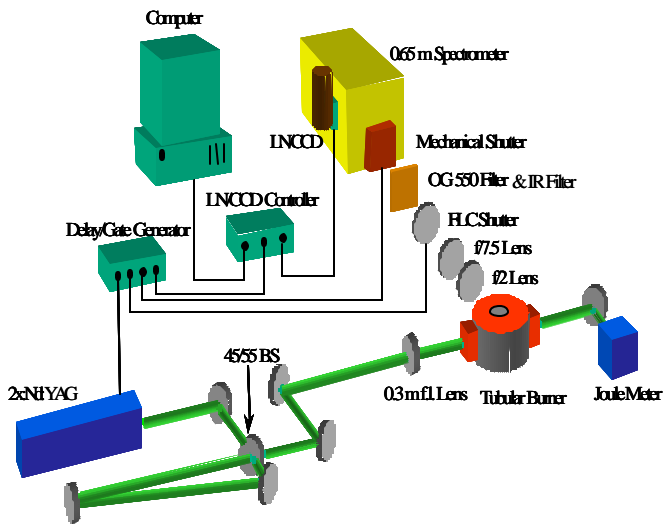


Fig. 2. Schematic of the Visible Raman setup.

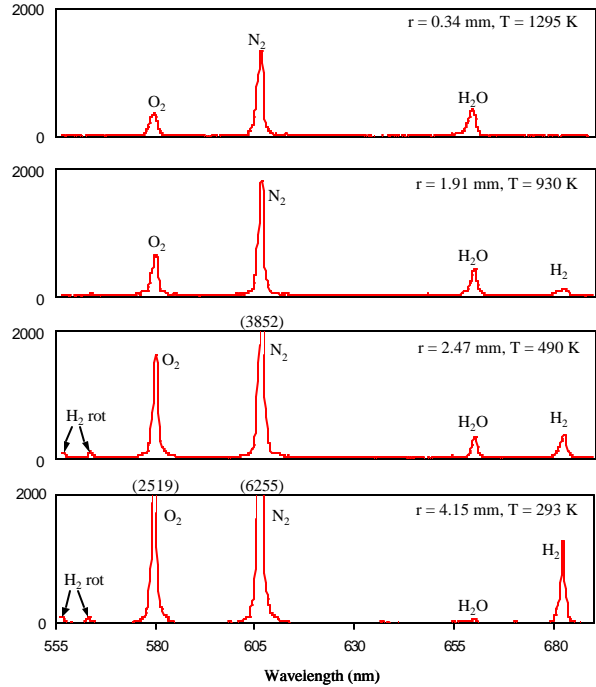


Fig. 3. Time-averaged, background subtracted, spectra from line-imaged Raman scattering in a laminar, premixed H_2 -air tubular flame ($\phi = 0.175$, $k = 104 \text{ s}^{-1}$). Spectra correspond to 4 radial positions from the stagnation centerline of the flame: burned gas, initial reaction, pre-heat, and unburned gas regions.

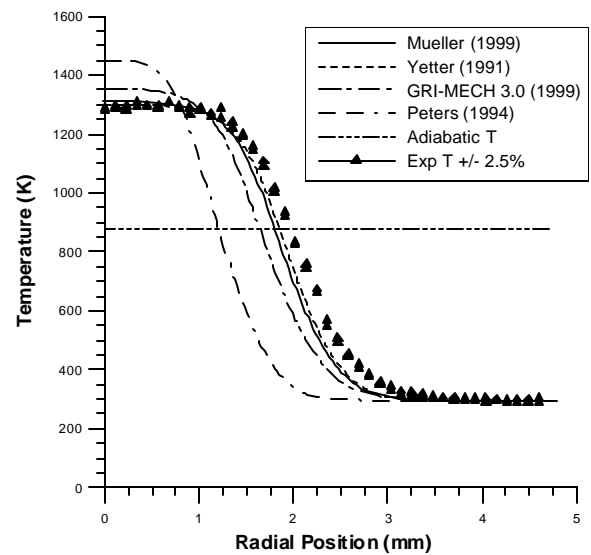


Fig. 4. Comparison of predicted temperature profiles from 4 reaction mechanisms in a premixed H_2 -air tubular flame ($\phi=0.175$, $k=90 \text{ s}^{-1}$).

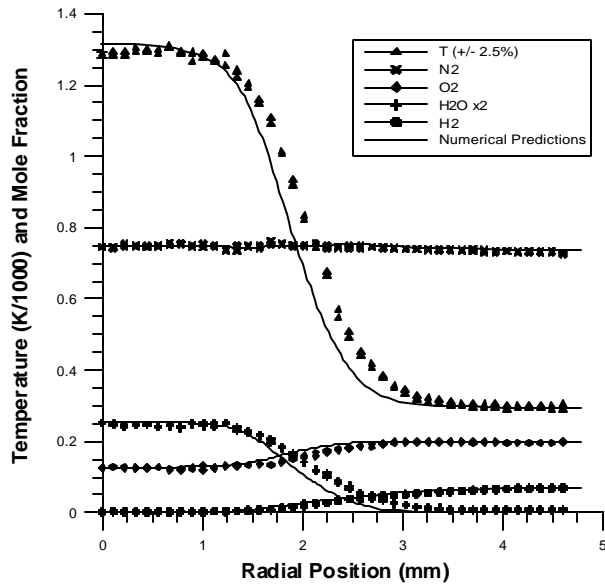


Fig. 5. Raman-derived and numerically-predicted product measurements using Mueller et al. chemistry with thermal diffusion in $\phi=0.175$, $k=90 \text{ s}^{-1}$ H_2 -air tubular flame.

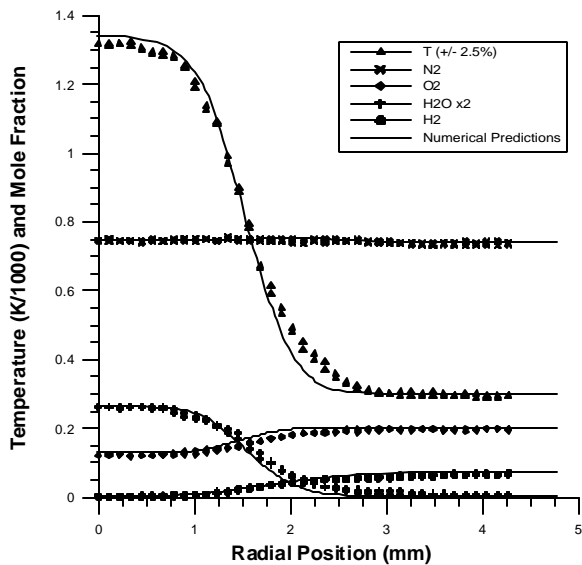


Fig. 6. Raman-derived and numerically-predicted product measurements using Mueller et al. chemistry with thermal diffusion in $\phi=0.175$, $k=127 \text{ s}^{-1}$ H_2 -air tubular flame.

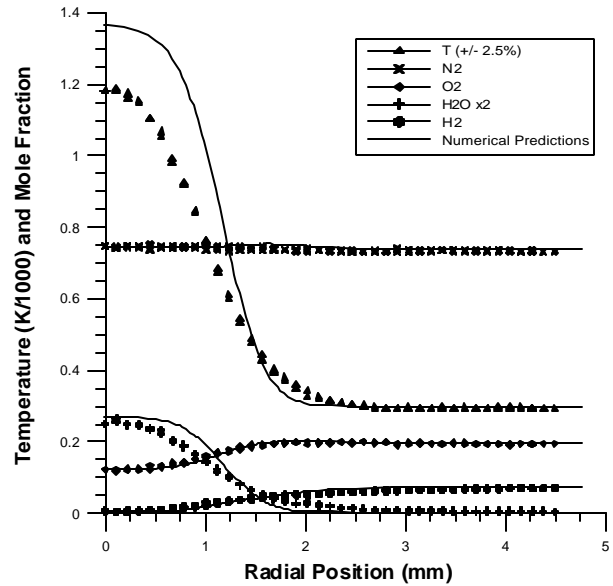


Fig. 7. Raman-derived and numerically-predicted product measurements using Mueller et al. chemistry with thermal diffusion in $\phi=0.175$, $k=190 \text{ s}^{-1}$ H_2 -air tubular flame.

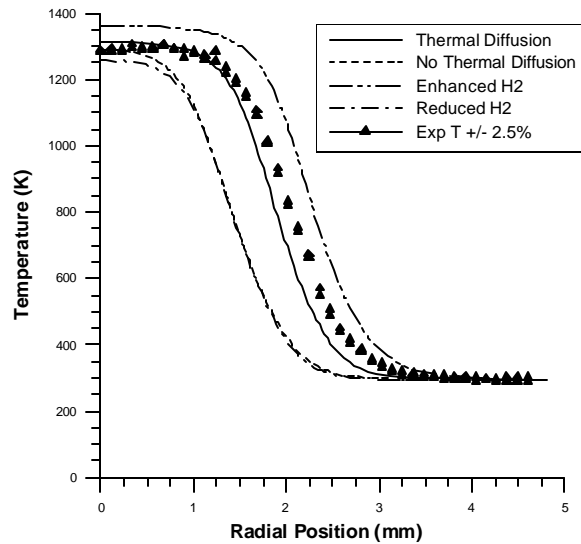


Fig. 8. Simulation using Mueller et al. chemistry showing effects of thermal diffusion coefficient and increasing/decreasing the binary diffusion coefficient of H_2 into N_2 by +32%/-29% in a H_2 -air tubular flame ($\phi = 0.175$, $k = 90 \text{ s}^{-1}$).

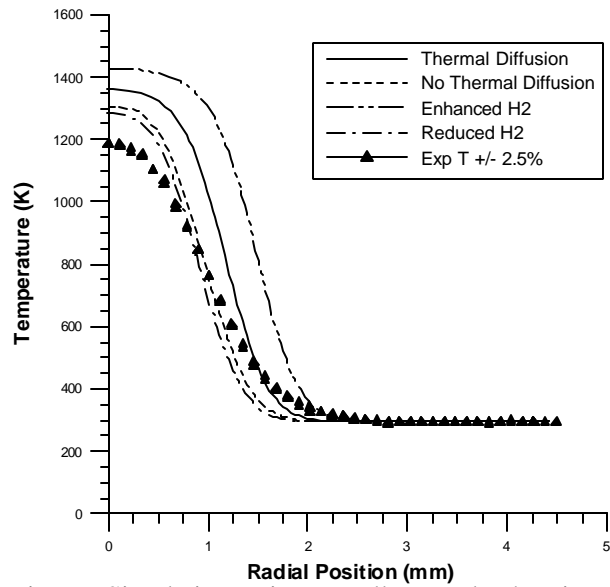


Fig. 9. Simulation using Mueller et al. chemistry showing effects of thermal diffusion coefficient and increasing/decreasing the binary diffusion coefficient of H_2 into N_2 by +32%/-29% in a H_2 -air tubular flame ($\phi = 0.175$, $k = 190 \text{ s}^{-1}$).

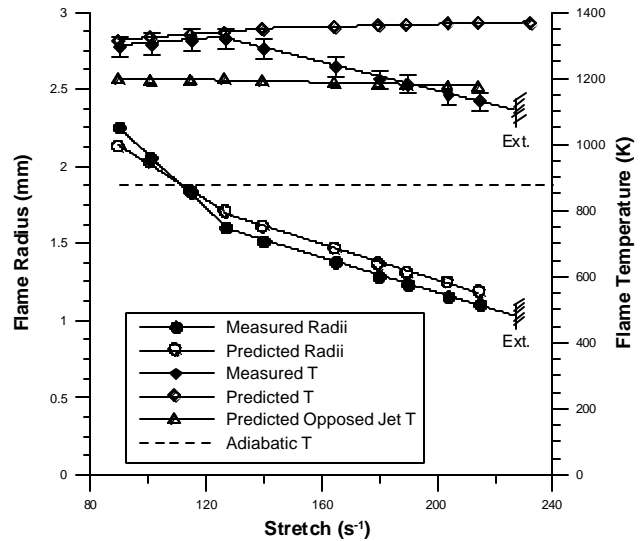


Fig. 10. Comparison of flame radius and peak flame temperature vs. stretch for H_2 -air tubular flames of $\phi = 0.175$. Numerical simulations of opposed jet flames under identical conditions are shown for comparison.